A Novel Experimental Search Channel
for Very Light Higgses in the 2HDM Type I

S. Moretti[1,2*], S. Semlali[1,3†], C. H. Shepherd-Themistocleous[3‡]

[1]*School of Physics and Astronomy, University of Southampton, Southampton, SO17 1BJ, UK*
[2]*Department of Physics & Astronomy, Uppsala University, Box 516, SE-751 20 Uppsala, Sweden*
[3]*Particle Physics Department, Rutherford Appleton Laboratory, Chilton, Didcot, Oxon OX11 0QX, UK*

Abstract

We present a reinterpretation study of existing results from the CMS Collaboration, specifically, searches for light Beyond the Standard Model (BSM) Higgs pairs produced in the chain decay $pp \to H_{\mathrm{SM}} \to hh(aa)$ into a variety of final states, in the context of the CP-conserving 2-Higgs Doublet Model (2HDM) Type-I. Through this, we test the Large Hadron Collider (LHC) sensitivity to a possible new signature, $pp \to H_{\mathrm{SM}} \to ZA \to ZZh$, with $ZZ \to jj\mu^+\mu^-$ and $h \to b\bar{b}$. We perform a systematic scan over the 2HDM Type-I parameter space, by taking into account all available theoretical and experimental constraints, in order to find a region with a potentially visible signal. We investigate the significance of it through a full Monte Carlo simulation down to the parametrised detector level. We show that such a signal is an alternative promising channel to standard four-body searches for light BSM Higgses at the LHC already with an integrated luminosity of $\mathcal{L} = 300$ fb^{-1}. For a tenfold increase of the latter, discovery should be possible over most of the allowed parameter space.

---

[*]s.moretti@soton.ac.uk, stefano.moretti@physics.uu.se
[†]souad.semlali@soton.ac.uk
[‡]claire.shepherd@stfc.ac.uk

1 Introduction

One of the main goals of the LHC machine is to investigate the individual properties (mass, width, spin, CP quantum numbers) and interactions (with both matter and forces) of the Higgs boson and to look into evidence for new physics. These Higgs features have been probed by the ATLAS and CMS collaborations, using proton-proton (pp) collision data collected at centre-of-mass energies of $\sqrt{s} = 7$ TeV, 8 TeV and 13 TeV for an integrated luminosity of 25 fb^{-1} up to 139 fb^{-1}. Although the measurements of the Higgs mass [1–3], spin [4], width [5, 6] and couplings to SM fermions and vector bosons [7–12] are all indeed in a good agreement with the SM theoretical predictions, the uncertainties on the SM-like Higgs couplings probed in multiple production modes for the five key decay channels $H \to \gamma\gamma$ [13–17], ZZ^* [16–18], WW^* [19–22], $\tau\tau$ [11, 22, 23] and $b\bar{b}$ [17, 24, 25] provide signs of a possible potential BSM contributions to the total Higgs width and hints of new physics through the invisible and/or undetected decays. It is worth highlighting that indirect constraints from the current fit of couplings measurements and direct searches for $H \to inv$ (i.e., to 'invisible' final states) performed by ATLAS and CMS collaborations have placed upper limits on the Branching Ratio (BR) of Higgs boson to invisible particles and undetected BSM particles at 95% C.L. (Confidence Level) [26–28].

Furthermore, the Higgs self-couplings are one of the most interesting interactions that can be probed at the LHC with sufficient luminosity, although, at present (i.e., at the end of Run 2), they are not determined yet. A measurement of this interaction is one of the highest priority goals during, possibly, Run 3 and, certainly, at the High Luminosity LHC (HL-LHC), both of which would, therefore, start shedding light on the nature of the Higgs boson and the shape of the Higgs potential, which in turn has implications for the vacuum metastability, the hierarchy problem as well as the strength of the Electro-Weak (EW) phase transition. However, probing Higgs self-interactions, both trilinear and quartic couplings, in multi-Higgs production is experimentally very challenging due to the small cross section for SM-like di-Higgs production via the gluon fusion process, even at Next-to-Next-to-Leading Order (NNLO) [29]. Both the ATLAS and CMS collaborations have set upper limits at 95% C.L. on the Higgs production cross sections after performing searches in various final states, e.g. $b\bar{b}\gamma\gamma$ [30,31], $b\bar{b}\tau\tau$ [32] and $b\bar{b}b\bar{b}$ [33,34]. From the theory side, many models with an extended scalar sector can be responsible for enhanced (SM-like) di-Higgs production, like the 2-Higgs Doublet model (2HDM), the Next-to-2HDM (N2HDM) and a variety if both minimal and non-minimal Supersymmetric (SUSY) models. In fact, all such BSM scenarios also present the additional features of new di-Higgs final states, as they all present with additional CP-even and/or -odd Higgs states, which can be accessible by the LHC experiments in a variety of signatures.

This paper focuses on the popular 2HDM. After EW Symmetry Breaking (EWSB), the scalar sector of the 2HDM predicts five physical Higgs states, two CP-even Higgses (h, H, with $m_h < m_H$), one CP-odd one (a) and a pair of charged ones ($H^\pm$). The rich (pseudo)scalar sector of the 2HDM and the different sets of Yukawa couplings that can be realised then offer a very interesting production and decay phenomenology of neutral and charged Higgs states at the LHC, even after scrutinising the 2HDM parameter space by considering different theoretical (vacuum stability, perturbativity, unitarity, etc.) and experimental (from SM-like Higgs data and nil searches for companion states, flavour physics and low energy observables, etc.) constraints. Furthermore, the 2HDM is also attractive because one can impose a simple Z_2 discrete symmetry to the Yukawa sector in order to suppress Flavour Changing Neutral Currents (FCNCs) at tree level, which then forces one doublet to couple to a given type of fermions and leading as a result to four Yukawa interactions (termed, Type-I, Type-II, Type-X and Type-Y). In fact, in order to realise EWSB in such a way that the 2HDM is compliant with all experimental data, it is finally customary to allow for a soft breaking of this Z_2 symmetry. Herein, we will use the latter setup with a Type-I Yukawa structure.

Specifically, in the present study, we plan to take advantage of the direct access to some trilinear Higgs couplings that the LHC can access, entering multi-Higgs processes such as $H \to hh(aa)$ and $H^{\pm} \to W^{\pm}a$, to search for light Higgs states in cascade (or chain) or decays in the framework of 2HDM Type-I. In fact, as the analysis progress, we aim to use the information and the strong correlation between the aforementioned couplings to explore the scope of a new search for light Higgses at the LHC Run 3 (with an integrated luminosity of 300 fb^{-1}) as well as the HL-LHC (with an integrated luminosity of 3000 fb^{-1}), on the basis of the knowledge acquired from the study of the aforementioned signatures. Chiefly, we focus on the case where H is the observed Higgs with a mass of 125 GeV, while h and a are lighter, which then opens a window for non SM-like Higgs decays, such as $H \to Z^{(*)}a$. This configuration is possible in a 2HDM Type-I, in turn offering the possibility of an alternative and new promising signal, in the form of the following cascade decays $H \to Z^*a \to Z^*Z^*h \to b\bar{b}\mu^-\mu^+jj$. The main Higgs production process is via gluon fusion $gg \to H$.

In what follows, we provide a brief review of the 2HDM Type-I, in section 2. Then, in section 3, we discuss the outcome of recasting the aforementioned cascade Higgs decays in such a framework. Section 4 is devoted to the signal-to-background analysis of the proposed new signal based on running a full Monte Carlo (MC) simulation while we finally conclude in section 5.

2 2HDM Type-I

The 2HDM is one of the simplest well-motivated extensions of the SM. In this section, we briefly review the theoretical structure of this model. The scalar sector of the 2HDM consists of two complex $SU(2)_L$ doublets, Φ_1 and Φ_2, with hypercharge $Y = +1$. The most general $SU(2)_L \times U(1)_Y$ invariant scalar potential can be written as follows:

$$
\begin{aligned}
V(\Phi_1, \Phi_2) &= m_{11}^2 \Phi_1^\dagger \Phi_1 + m_{22}^2 \Phi_2^\dagger \Phi_2 - [m_{12}^2 \Phi_1^\dagger \Phi_2 + \text{h.c.}] \\
&+ \frac{\lambda_1}{2}(\Phi_1^\dagger \Phi_1)^2 + \frac{\lambda_2}{2}(\Phi_2^\dagger \Phi_2)^2 + \lambda_3(\Phi_1^\dagger \Phi_1)(\Phi_2^\dagger \Phi_2) + \lambda_4(\Phi_1^\dagger \Phi_2)(\Phi_2^\dagger \Phi_1) \\
&+ \left\{ \frac{\lambda_5}{2}(\Phi_1^\dagger \Phi_2)^2 + \left[\lambda_6(\Phi_1^\dagger \Phi_1) + \lambda_7(\Phi_2^\dagger \Phi_2)\right] \Phi_1^\dagger \Phi_2 + \text{h.c.} \right\}.
\end{aligned}
\tag{1}
$$

Assuming CP-conservation in the 2HDM and following the hermiticity of the scalar potential, m_{11}^2, m_{22}^2, m_{12}^2, $\lambda_{1,2,3,4,5,6}$ are real parameters. Invoking the described Z_2 symmetry, to avoid tree-level Higgs-mediated FCNCs at tree level, implies that $\lambda_6 = \lambda_7 = 0$. Also notice that the bilinear term proportional to m_{12}^2 breaks the Z_2 symmetry softly. Using the two minimisation conditions of the scalar potential and the combination $v^2 = v_1^2 + v_2^2 = (2\sqrt{2}G_F)^{-1}$, one can then trade the Lagrangian parameters of the 2HDM for a more convenient set of variables,

$$
\alpha, \ \tan\beta = \frac{v_2}{v_1}, \ m_h, \ m_H, \ m_a, \ m_{H^\pm} \quad \text{and} \quad m_{12}^2,
$$

where α is the CP-even mixing angle, v_1 and v_2 are the Vaccum Expectations Values (VEVs) of the two Higgs doublets Φ_1 and Φ_2, respectively.

2.1 Yukawa couplings

The general structure of the Yukawa Lagrangian when both Higgs fields couple to all fermions is given by:

$$
\mathcal{L}_Y = \bar{Q}'_L(Y_1^u \tilde{\Phi}_1 + Y_2^u \tilde{\Phi}_2)u'_R + \bar{Q}'_L(Y_1^d \Phi_1 + Y_2^d \Phi_2)d'_R + \bar{L}'_L(Y_1^l \Phi_1 + Y_2^l \Phi_2)l'_R + \text{h.c.},
\tag{2}
$$

where Q'_L and L'_L are the weak isospin quark and lepton doublets, u'_R and d'_R denote the right-handed quark singlets while $Y^u_{1,2}$, $Y^d_{1,2}$ and $Y^l_{1,2}$ are couplings matrices in flavour space. This form of Yukawa interaction gives rise to large FCNCs at tree level, which is strongly constrained by B-physics observables. Implementing Z_2 symmetry allows only one doublet to couple to a given right-handed fermion field. Depending on the Z_2 assignment, one can have the four types of models previously refered to as Type-I, Type-II, Type-X and Type-Y. In the mass-eigenstate basis, they can be unified and expressed as follows:

$$-\mathcal{L}_Y = + \sum_{f=u,d,\ell} \left[m_f \bar{f}f + \left(\frac{m_f}{v}\kappa^f_h \bar{f}fh + \frac{m_f}{v}\kappa^f_H \bar{f}fH - i\frac{m_f}{v}\kappa^f_A \bar{f}\gamma_5 fA \right) \right]$$
$$+ \frac{\sqrt{2}}{v}\bar{u}\left(m_u V\kappa^u_A P_L + V m_d \kappa^d_A P_R \right) dH^+ + \frac{\sqrt{2}m_\ell \kappa^\ell_A}{v}\bar{\nu}_L \ell_R H^+ + \text{h.c.}, \tag{3}$$

where $P_{L,R} = (1 \pm \gamma_5)/2$ are the projection operators and V denotes the Cabibbo-Kobayashi-Maskawa (CKM) matrix.

Here, we focus only on Type-I, where only one doublet Φ_2 couples to all fermions, and thus the Higgs-fermion couplings are flavour diagonal in the fermion mass basis and depend only on the mixing angles, α and β, as follows:

$$\kappa^{u,\,d,\,l}_h = c_\alpha/s_\beta = s_{\beta-\alpha} + \cot\beta\, c_{\beta-\alpha}, \tag{4}$$
$$\kappa^{u,\,d,\,l}_H = s_\alpha/s_\beta = c_{\beta-\alpha} - \cot\beta\, s_{\beta-\alpha}, \tag{5}$$
$$\kappa^{d,\,l}_A = -\cot\beta, \quad \kappa^u_A = \cot\beta, \tag{6}$$

where we have used the short-hand notation c and s for cos and sin, respectively.

2.2 Theoretical and Experimental Constraints

We now describe briefly a set of, in turn, theoretical and experimental constraints that must be satisfied by the parameter space of the 2HDM.

- Perturbative unitarity [35–37] forces several constraints on the quartic couplings of the scalar potential by requiring the following inequalities:

$$\frac{3}{2}\left\{ (\lambda_1 + \lambda_2) \pm \sqrt{(\lambda_1 - \lambda_2)^2 + \frac{4}{9}(2\lambda_3 + \lambda_4)^2} \right\} < 8\pi, \quad (\lambda_3 \pm \lambda_5) < 8\pi, \tag{7}$$

$$\frac{1}{2}\left\{ (\lambda_1 + \lambda_2) \pm \sqrt{(\lambda_1 - \lambda_2)^2 + 4\lambda_4^2} \right\} < 8\pi, \quad (\lambda_3 + 2\lambda_4 \pm 3\lambda_5) < 8\pi, \tag{8}$$

$$\frac{1}{2}\left\{ (\lambda_1 + \lambda_2) \pm \sqrt{(\lambda_1 - \lambda_2)^2 + 4\lambda_5^2} \right\} < 8\pi. \tag{9}$$

- Vacuum stability [38] requires the scalar potential to be finite at large field values and this can be translated into these bounds:

$$\lambda_{1,2} > 0, \ \lambda_3 > -\sqrt{\lambda_1\lambda_2}, \ \lambda_3 + \lambda_4 - |\lambda_5| > -\sqrt{\lambda_1\lambda_2}. \tag{10}$$

- Perturbativity requires the quartic couplings to obey $|\lambda_i| < 4\pi$ $(i = 1, \ldots, 5)$.

Experimental observations impose the following constraints:

- EW precision observables, i.e., the oblique parameters, S, T and U [39, 40] are required to be within 95% C.L. of their experimental measurements, the current fit values (with the correlation parameters) are given by [41]:

$$S = -0.01 \pm 0.10, \quad T = 0.03 \pm 0.12, \quad U = 0.02 \pm 0.11,$$
$$\rho_{ST} = 0.92, \quad \rho_{SU} = -0.80, \quad \rho_{TU} = -0.93, \quad \chi_{ST,\ SU,\ TU} < 5.99.$$

The above constraints have been implemented in 2HDMC-1.8.0 [42]. This public code is then used to scan over the parameter space of the 2HDM and test it against the above contraints as well as to compute the different Higgs BRs in each point of it. (2HDMC also provides an interface to HiggsBounds and HiggsSignals, see below.)

Further experimental observations are utlized as follows:

- Consistency with the Z width measurement $\Gamma_Z = 2.4952 \pm 0.0023$ GeV from LEP [41] is required.

- Constraints from LHC, Tevatron and LEP searches which failed to find companion Higgs states are taken into account via HiggsBounds-5.10.0 [43], which allows to test the exclusion limits at 95% C.L.

- The code HiggsSignals-2.6.2 [44] is used to check the signal strength measurements of the SM-like Higgs boson discovered at the LHC in 2012.

- Constraints from B-physics observables are enforced by Superiso-v1.4 [45], using the following measured observables:

$$\mathrm{BR}(B_d \to \mu^+\mu^-) = (3.9 \pm 1.5) \times 10^{-4} \ \ [46], \qquad \mathrm{BR}(B_s \to \mu^+\mu^-) = (3.0 \pm 0.6) \times 10^{-9} \ \ [47],$$
$$\mathrm{BR}(B \to X_s\gamma) \ = \ (3.32 \pm 0.15) \times 10^{-3} \ \ [48].$$

- Constraints from recent searches for light pseudoscalar states in the mass range [15, 62.5] GeV, in proton-proton collision at $\sqrt{s} = 13$ TeV, in $2\mu2b$ [49, 50], $2\tau2\mu$ [51] and $2b2\tau$ [52] final states, are included in HiggsBounds. Since no significant excess is observed, upper limits are set on $\mathrm{BR}(H \to aa \to 2\mu2b,\ 2\mu2\tau,\ 2b2\tau)$ [49, 51, 52]. However, lately, additional constraints from such Higgs cascade decays have emerged, not included in the numerical tool, so we had to deal with these separately. For example, the CMS group has reported a search for $H \to aa \to 4\gamma$ [53], using the data collected at $\sqrt{s} = 13$ TeV, with an integrated luminosity of 132 fb^{-1}. Upper limits can then be set on $\mathrm{BR}(H \to aa \to 4\gamma)$ at 95% C.L, since no significant deviation is observed[1]. The ATLAS group [56] has also recently searched for the exotic decay of the Higgs boson into two light pseudoscalars in $2b2\mu$ final state at $\sqrt{s} = 13$ TeV with an integrated luminosity of 137 fb^{-1}, in the range of masses varying from 15 GeV to 60 GeV. (The largest excess with a local significance of 3.3σ is observed at a dimuon invariant mass of 52 GeV.) In the background only hypothesis, upper limits at 95% C.L. can be placed on $\mathrm{BR}(H \to aa \to 2b2\mu)$[3]. Tab. 1 summarises several searches for exotic decays of the Higgs bosons in various final states, performed by the two collaborations ATLAS and CMS at Run 2, targeting a different ranges of masses.

---

[1]EasyNData [54] was used to digitise the exclusion limits from the published papers in order to test each point in the parameter space against the upper limit on $\mathrm{BR}(H \to hh(aa) \to 4\gamma)$ [53], a procedure which was validated against the case of $\mathrm{BR}(H \to hh(aa) \to 2\mu2\tau)$ using [55].

[3]Corresponding search data and exclusion limits are available at the HEPData database.

Limit	Collaboration	Range	HiggsBounds
$S \to HH \to 2b2\gamma$ [30]	CMS	$250\text{GeV} < m_S < 900$	×
$S \to HH \to 2b2\tau$ [32]	CMS	$250\text{GeV} < m_S < 900\text{GeV}$	×
$H \to aa \to 2b2\mu$ [49]	CMS	$15\text{GeV} < m_a < 60\text{GeV}$	✓
$H \to aa \to 2b2\mu$ [50]	ATLAS	$15\text{GeV} < m_a < 60\text{GeV}$	✓
$H \to aa \to 2\mu2\tau$ [51]	CMS	$15\text{GeV} < m_a < 61.5\text{GeV}$	✓
$H \to aa \to 2b2\tau$ [52]	CMS	$15\text{GeV} < m_a < 60\text{GeV}$	✓
$H \to aa \to 4\gamma$ [53]	CMS	$15\text{GeV} < m_a < 60\text{GeV}$	×
$H \to aa \to 2\mu2\tau$ [55]	CMS	$3.6\text{GeV} < m_a < 21\text{GeV}$	×
$H \to aa \to 2b2\mu$ [56]	ATLAS	$15\text{GeV} < m_a < 60\text{GeV}$	×
$S \to HH \to bbVV$ [57], [58]	CMS	$260\text{GeV} < m_S < 900\text{GeV}$	✓
$H \to aa \to 4b$ [59]	ATLAS	$20\text{GeV} < m_a < 60\text{GeV}$	✓
$S \to HH \to 2b2\gamma$ [60]	ATLAS	$260\text{GeV} < m_S < 1000$	✓
$S \to HH \to 2b2\gamma$ [61]	ATLAS	$250\text{GeV} < m_S < 1000$	×

Table 1: (×)/(✓) indicate searches (not yet)/(already) implemented in `HiggsBounds-5.10.0`.

3 Numerical Analyses

The (pseudo)scalar sector of the 2HDM involves two CP-even Higgses, h and H. One of these scalars can be identified as the 125 GeV state observed at the LHC. As mentioned, in this analysis, we will assume that the heaviest Higgs state H is the SM-like one with a mass of 125 GeV and that h and a are lighter than H. We the perform a scan over the following ranges,

$$m_h \in [10 \text{ GeV}, \ 90 \text{ GeV}], \quad m_H = 125 \text{ GeV}, \quad m_a \in [10 \text{ GeV}, \ 90 \text{ GeV}],$$
$$m_{H^\pm} \in [100 \text{ GeV}, \ 160 \text{ GeV}], \quad \tan\beta \in [2.5, \ 25], \quad \sin(\beta - \alpha) \in [-0.7, \ 0.0],$$

with $m_{12}^2 = m_a^2 \tan\beta/(1 + \tan^2\beta)$. Assuming $m_H = 125$ GeV and $m_{h,a} < 90$ GeV, the decay channels $H \to hh, aa, \ aZ^*$ could be open, leading to invisible or undetected SM-like Higgs decays that are restricted by the current precision measurements of Higgs couplings. CMS performed a combination of searches, using data collected at $\sqrt{s} = 7, \ 8, \ 13$ TeV [27], for Higgs bosons decaying into invisible particles, which targets the following production channels: Vector Boson Fusion (VBF), Higgs-Strahlung (HS) and gluon-gluon Fusion (ggF) (allowing for initial state radiation). The combination of all the searches, assuming these SM-like production modes, yields an observed (expected) upper limit on BR($H \to inv$) of 0.19 (0.15) at 95% C.L. The ATLAS group reported a direct search for Higgs bosons produced via VBF with subsequent invisible decays, for 139 fb^{-1} of pp collision data at $\sqrt{s} = 13$ TeV [28]. An observed (expected) upper limit of 0.145 (0.103) is placed on BR($H \to inv$) at 95% C.L., as a function of the assumed production cross sections. In our analysis, we will assume that BR($H \to inv$) designates the sum of the following decay rates, BR($H \to hh$), BR($H \to aa$) and BR($H \to aZ^*$).

After performing a random scan over 2HDM Type-I parameters, we show in Fig. 1 the region allowed by theoretical and experimental constraints. Within this region the most sensitive channels to the parameter space of the model as determined by `HiggsBounds` are shown by coloured dots. Obviously, there are two distinct regions in the figure. The one in the top left corner corresponds to low masses of h ($m_h < m_H/2$), and high masses of a ($m_a > m_H/2$), while the second one corresponds to the $m_{a, \ h} > m_H/2$ scenario. It is interesting to note that there are no acceptable
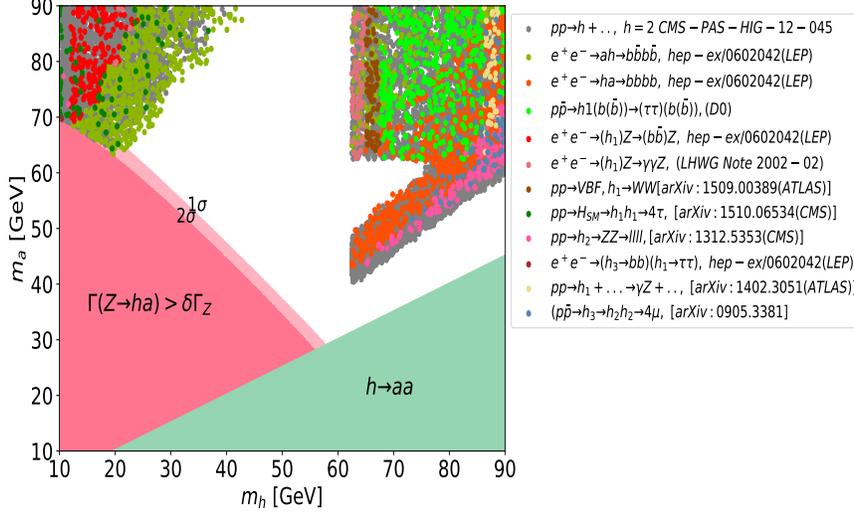
Figure 1: Allowed parameter space in the 2HDM Type-I at 95% C.L. Coloured dots represent the searches to which the relevant (m_h, m_a) regions are sensitive to.

points when 40 GeV $< m_h < m_H/2$ and $m_a > m_H/2$. This is due to the fact that this parameter combination is excluded by LEP searches for $e^+e^- \to ah \to b\bar{b}b\bar{b}$ [62] and an ATLAS search for events with at least 3γ in $pp \to H_{\rm SM} \to hh \to 4\gamma$ [63]. The figure also captures the constraints from the Z width, which forbid possible mass combinations (m_h, m_a) when $\cos(\beta-\alpha) \to 1$. Additionally, the constraint from the LEP search for the $e^+e^- \to (h \to aa)a \to (b\bar{b}b\bar{b})b\bar{b}$ process [62] excludes the bottom right region corresponding to $m_h > 2m_a$, where the decay channel $h \to aa$ is kinematically open.

Finally, an interesting observation is that the sensitivity in the region with low m_h and high m_a is mainly from LEP searches for processes such as $e^+e^- \to ah \to b\bar{b}b\bar{b}$ and $e^+e^- \to (h)Z \to (b\bar{b})Z$ [62]. Therefore, an update from the LHC during Run 3 is unlikely to rule out this mass combination over the plane (m_h, m_a) of the 2HDM Type-I. We will be focusing on this region in the second part of our study.

We now turn to the reinterpretation of exotic Higgs decay searches, i.e., $H \to aa$ in $2b2\tau$, $2b2\mu$ and $2\mu2\tau$ final states in the framework of the 2HDM Type-I, while taking advantage of the parameter space discussed above. The recasting of $2b2\tau$, $2b2\mu$ and $2\tau2\mu$ searches for $H \to hh$ is also possible since these processes share similar kinematics (in the same spirit as in Ref. [64]). It is relevant to note that the constraints from the search for light pseudoscalars in the $2b2\tau$ final state are much stronger than the ones from $2b2\mu$ and $2\tau2\mu$ searches. CMS has set an upper limit, between 3% and 12%, on BR($H \to aa \to 2b2\tau$) at 95% C.L. [52], assuming the SM production of primary Higgs boson. We show in Fig. 2 the outcome from reinterpreting the $H \to aa(hh) \to 2b2\tau$ search in the 2HDM Type-I. Grey points satisfy theoretical constraints as described in section 2.2, whereas red points are excluded by nil searches (i.e., by `HiggsBounds`). The area of sensitivity to $H \to aa(hh) \to 2b2\tau$ is excluded. The blue points satisfy both theoretical and experimental constraints. In this connection, the BR of Higgs SM-like Higgs state decaying into hh and/or aa is very restricted and cannot exceed 9% at 95% C.L., again, in the 2HDM Type-I. One can draw a similar conclusion form reinterpreting $H \to hh(aa) \to 2b2\mu$ in our reference framework. Fig. 3 shows that the parameter space with sensitivity to this search is excluded . One should keep in mind that the $2b2\mu$ final state is well-balanced between large BR($h/a \to b\bar{b}$) and a clean di-muon resonance that is easy to trigger on. This exercise emphasises that the 2HDM Type-I may not be a good framework for reinterpreting searches for exotic Higgs decays into light pseudoscalar in
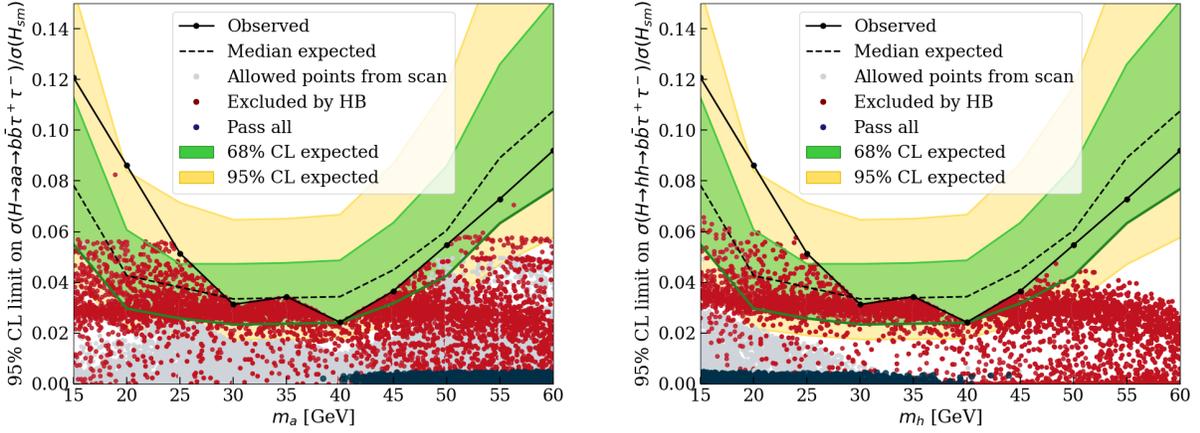
Figure 2: Observed and expected upper limits on $\sigma(H \to aa(hh) \to b\bar{b}\tau^+\tau^-)/\sigma_{\text{SM}}(H)$ [52] at 95% C.L. in the 2HDM Type-I. Grey points are allowed by theoretical constraints. Blue points satisfy both theoretical and experimental constraints
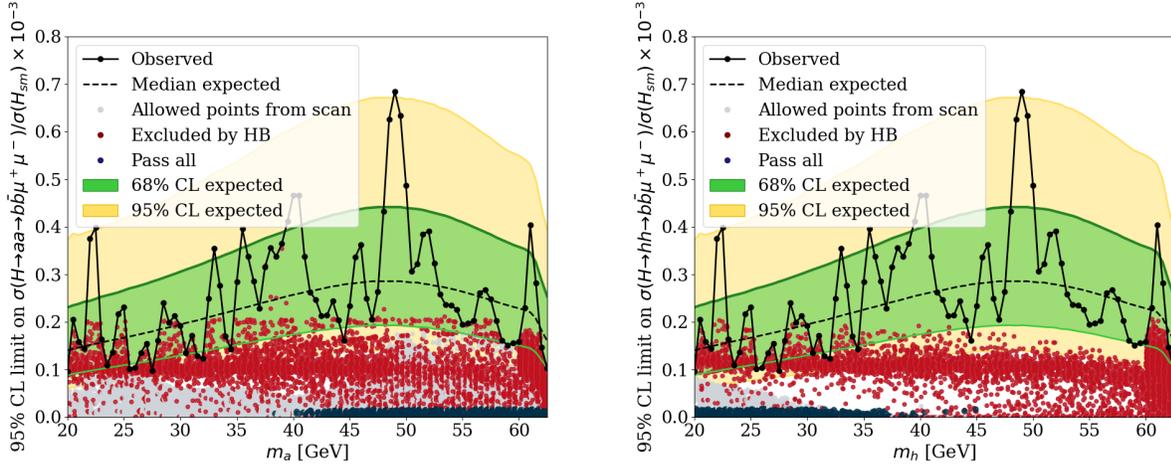
Figure 3: Observed and expected upper limits on $\sigma(H \to aa(hh) \to b\bar{b}\mu^+\mu^-)/\sigma_{\text{SM}}(H)$ [49] at 95% C.L. in the 2HDM Type-I.

"traditional" final states such as $2b2\mu$, $2b2\tau$ and $2\tau2\mu$. We also address here light charged Higgs decay in the mass ranges where $m_{H^\pm} < m_t - m_b$ and $m_{h,a} < 90$ GeV. In this configuration, the charged Higgs state can be be produced from top quark decays, i.e., $t \to bH^+$, followed by its bosonic decays to $H^\pm \to W^\pm h(a)$, instead of the standard fermionic decay modes like $\tau\nu$ and cs. Many studies motivated these channels as alternative modes to search for light charged Higgs bosons that could dominate over the conventional fermionic channels, because of large BRs when they are kinematically allowed, in models such as our 2HDM Type-I [65–67]. ATLAS [68] and CMS [69] have considered the ranges $m_a \in [15, 75]$ GeV and $m_{H^\pm} < m_t - m_b$ to search for light charged Higgs bosons in $pp \to t\bar{t} \to b\bar{b}H^+W^-$ with $H^+ \to W^+a$ and $a \to \mu^+\mu^-$ at $\sqrt{s} = 13$ TeV, since the $\mu^+\mu^-$ finale state provides the aforementioned experimental advantages, which offset the suppressed rate of $\text{BR}(a \to \mu^+\mu^-)$. Previously, both CDF and the LEP collaborations have searched for $H^\pm \to W^\pm a$ with $a \to b\bar{b}$ [70], $a \to \tau^+\tau^-$ [71] and $a \to b\bar{b}$ [72]. In addition, LEP

experiments [73] have set a lower bound on the charged Higgs boson mass of $m_{H^\pm} > 72.5$ GeV in the 2HDM Type-I for $m_a > 12$ GeV at 95% C.L.
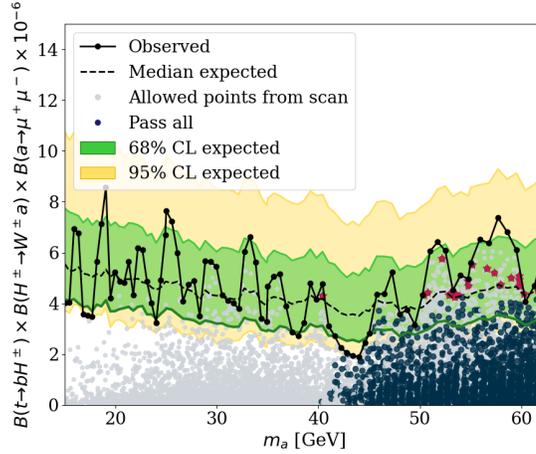
Figure 4: Observed and expected upper limits on $\mathrm{BR}(t \to H^+b) \times \mathrm{BR}(H^+ \to W^+a) \times \mathrm{BR}(a \to \mu^+\mu^-)$ [69] at 95% C.L. in the 2HDM Type-I.

Fig. 4 shows the CMS observed and expected exclusion limits on the product of the BRs of $t \to bH^\pm$, $H^\pm \to W^\pm a$ and $a \to \mu^+\mu^-$ [69] as a function of m_a predicted by the 2HDM Type-I, with respect to several theoretical and experimental constraints. We adopt here $m_{H^\pm} = m_a + 85$ GeV [69], which enables us to consider $H^\pm \to W^{\pm(*)}a$, with $W^{\pm(*)}$ being on/off shell, by randomly sampling values of the charged Higgs mass between 100 GeV and 160 GeV (see Eq. (11)). The yellow and green bands represent the uncertainties at $\pm 1\sigma$ and $\pm 2\sigma$ associated with the expected exclusion limits. An interesting observation is that the 2HDM Type-I offers sufficient sensitivity, when the prediction of the model exceeds the expected limit produced at $\sqrt{s} = 13$ TeV with an integrated luminosity of 35.9 fb^{-1} (purple stars). Such a signature could be exploited to search for a light $H^\pm$ at future experiments, Run 3 and/or the HL-LHC, given the available energies and luminosities by then. Therefore, we present in Tab. 2 some Benchmark Points (BPs) to test the actual sensitivity of these experiments to the 2HDM Type-I parameter space. In particular, we

Parameters	BP1	BP2	BP3	BP4
	(Masses are in GeV)			
m_h	62.86	75.69	75.58	77.18
m_H	125	125	125	125
m_a	40.37	50.73	52.90	53.44
$m_{H^\pm}$	105.19	108.15	110.83	111.95
$\tan\beta$	4.82	4.73	4.58	4.57
$\sin(\beta - \alpha)$	-0.203	-0.209	-0.220	-0.0215
	Total decay width in GeV			
$\Gamma(h)$	1.9×10^{-6}	3.00×10^{-6}	1.9×10^{-6}	3.00×10^{-6}
$\Gamma(H)$	4.54×10^{-3}	4.53×10^{-3}	4.47×10^{-3}	4.48×10^{-3}
$\Gamma(A)$	5.39×10^{-5}	6.79×10^{-5}	7.6×10^{-5}	7.7×10^{-5}
$\Gamma(H^\pm)$	3.31×10^{-4}	3.330×10^{-4}	3.339×10^{-4}	3.339×10^{-4}
	$\mathrm{BR}(A \to XY)$			
$\mathrm{BR}(A \to \mu\mu)$	2.36×10^{-4}	2.42×10^{-4}	2.43×10^{-4}	2.43×10^{-4}
	$\mathrm{BR}(H^\pm \to XY)$ in %			
$\mathrm{BR}(H^\pm \to W^+A)$	86.65	90.64	88.47	89.39

Table 2: BPs in the 2HDM Type-I.

move now to discuss a new analysis, where we deploy the parameter space of the 2HDM Type-I

following the outcomes of reinterpreting previous searches for light Higgses, $pp \to H_{\text{SM}} \to hh(aa)$, in different final states, in order to search for a new signature.
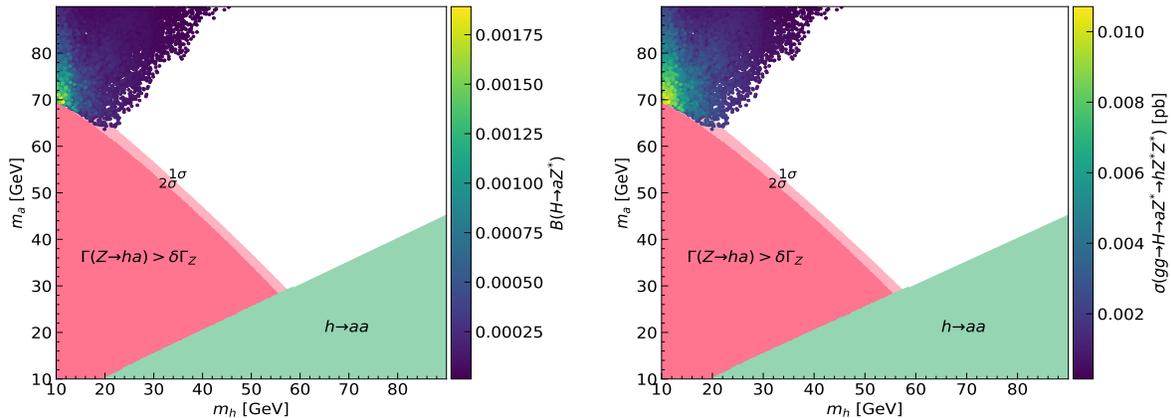
Figure 5: m_h and m_a vs. $\text{BR}(H \to Z^*a)$ (left) and $\sigma(gg \to H \to Z^*a \to Z^*Z^*h)$ (right) at 95% C.L. in the 2HDM Type-I.

Fig. 5 shows the result of performing a scan over the parameter space of 2HDM Type I, wherein (recall) the heaviest Higgs state is identified as the discovered SM-like one. Each sampled point is required to satisfy the theoretical and experimental constraints described in section 2.2. In the left panel, we illustrate m_a vs. m_h with the BR of $H \to aZ^{(*)}$ on the colour gauge. Since $m_H/2 < m_a < 125$ GeV, $H \to aZ^{(*)}$ will proceed with Z being off-shell, which explains the suppressed BR ($< 0.2\%$). In this configuration, $H \to aa$ will not be open, thus, $H \to hh$ would only contribute significantly to the undetected decays of H. It should be pointed out that the total amount of $\text{BR}(H \to aa^* + aZ^* + hh)$ should not exceed 19% as required by $\text{BR}(H \to inv)$. In the right panel, we show m_a as a function of m_h with $\sigma(H \to aZ^* \to hZ^*Z^* \to Z^*Z^*)$ on the colour gauge. Once the decay chain $H \to aZ^*$ is open, the subsequent decay of a could lead to $a \to Z^*h$ with Z being off-shell and h decaying to fermions and/or $\gamma\gamma$. We use Sushi [74–76] to compute the cross section of Higgs production at LO[2].

We show in Fig. 6 the $gg \to H \to aZ^* \to hZ^*Z^*$ cross section, where $h \to b\bar{b}$. The process could yield a cross section of 0.006 pb. In the right panel of Fig. 6 we show the BR of $h \to b\bar{b}$ in this region of the 2HDM Type-I parameter space. Obviously, the decay width of h is dominated by the decay mode $h \to b\bar{b}$. Thus, in what follows, we focus on the case where h decays to $b\bar{b}$ and $Z^{(*)}Z^{(*)} \to \mu^+\mu^- jj$. Such a scenario could be an alternative channel to search for light Higgses at Run 3 and the HL-LHC.

4 Signal vs. Background Analysis

We describe here the toolbox used to generate and analyse MC events. MadGraph-v.9.2.5 [77] is used to generate parton level configurations of both signal and background processes[3]. The events

---

[2]The signal cross sections is computed at LO (i.e, tree level) here, however, we will consider QCD corrections through K-factors later on in our study.

[3]Background and signal events are generated at LO. Higher order corrections are quantified through K-factors. The NLO QCD correction to top pair production in association with 2 jets computed at the LHC is about -27% [78], which we adopt here. The NLO corrections to $gg \to H$ are very large , about a facor of 2, due to the contributions from gg pairs to QCD radiation, whereas $K_{\text{NNLO/NLO}} \approx$ is much smaller than $K_{\text{NLO/LO}}$, signifying a convergence of the QCD expansion, so we renormalise the signal to the NNLO rates through the K-factor $K_{\text{NNLO/LO}} = \sigma^{\text{NNLO}}/\sigma^{\text{LO}} \sim 2.6-2.7$.
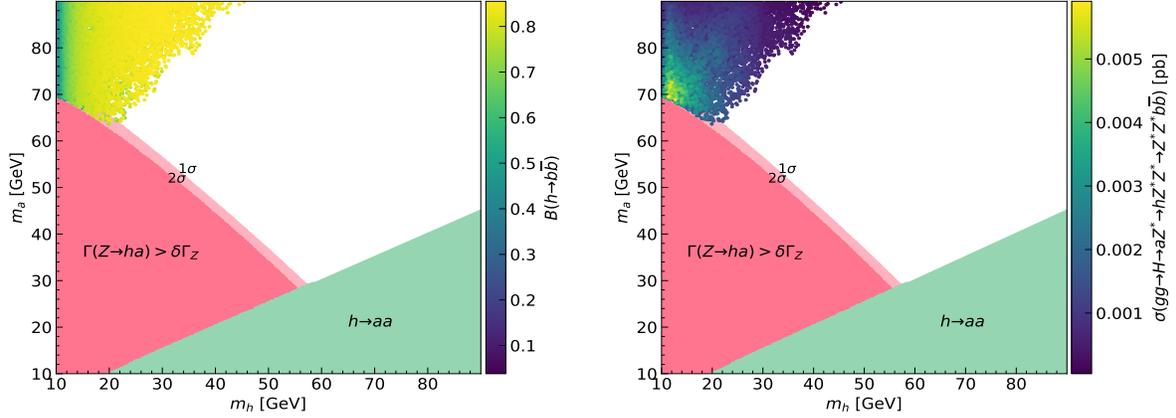
Figure 6: m_h and m_a vs. BR($h \to b\bar{b}$) (left) and $\sigma(gg \to H \to aZ^* \to hZ^*Z^* \to Z^*Z^*b\bar{b})$ (right) at 95% C.L. in the 2HDM Type-I.

are passed then to `PYTHIA8` [79] to simulate parton showering, hadronization and decays. Finally, we use `Delphes-3.5.0` [80] with the standard CMS card[4] to perform detector simulation. We resort to `MadAnalysis` [81] to apply cuts and to conduct the analysis. Background processes with dominant contributions are top pair production in association with 2 Initial State Radiation (ISR) jets[5] and ZZ production with additional $b\bar{b}$ quarks. We show in Tab. 3 the corresponding cross sections at $\sqrt{s} = 13$ TeV for the LHC energy. We have generated MC samples of $O(10^6)$ events. Unsurprisingly, the irreducible background $pp \to Z^{(*)}Z^{(*)}b\bar{b} \to b\bar{b}jj\mu^+\mu^-$ (from both QCD and EW interactions) is negligible whereas $pp \to ggt\bar{t} \to gg\mu^+\mu^-jjb\bar{b}\nu_\mu\bar{\nu}_\mu$ is large.

Background	Cross section (pb)
$pp \to ZZb\bar{b}_{\text{QCD}} \to \mu^+\mu^-jjb\bar{b}$	$9.27 \times 10^{-3} \pm 2.4 \times 10^{-5}$
$pp \to ZZb\bar{b}_{\text{QED}} \to \mu^+\mu^-jjb\bar{b}$	$2.42 \times 10^{-4} \pm 5.5 \times 10^{-7}$
$pp \to ggt\bar{t} \to gg\mu^+\mu^-jjb\bar{b}\nu_\mu\bar{\nu}_\mu$	2.92 ± 0.008

Table 3: The parton level cross sections of the background processes at LO.

We considered a few BPs for the signal given by $gg \to H \to aZ^* \to hZ^*Z^* \to \mu^+\mu^-\ jj\ b\bar{b}$ to perform the MC simulation. The input parameters of each BP are given in Tab. 4. Note that the light Higgs width, $\Gamma(h)$, is not small enough to lead to a large lifetime and hence, long-lived particles producing displaced vertices inside the detector. The proper decay length $c\tau_0$ is in fact only a tiny fraction of micrometers[6]. The different kinematic distributions at parton level in Fig. 7 show that the requirement of central pseudorapidity of the muons is generally satisfied however the p_T of these can be rather small, so that we will invoke the CMS di-muon trigger of Ref. [83], whereby the threshold is 17 GeV [83] for the muon with highest p_T and 8 GeV for the other. Fig. 8 shows the invariant mass distributions of the two b-jets, $m_{b\bar{b}}$, and that of the full final state, $m_{jj\mu^+\mu^-b\bar{b}}$, for the signal and the irreducible background processes at parton level, noting that $m_{b\bar{b}}$ is close to light Higgs mass m_h and $m_{jj\mu^+\mu^-b\bar{b}}$ is close to SM-like Higgs mass m_H (for the signal,

---

[4]It adopts the anti-k_T algorithm to cluster final particles into jets, with jet parameter $\Delta R = 0.5$ and $p_{T,j}^{\min} = 20$ GeV (for both light- and b-quark jets).

[5]In our study, we focus mainly on $ggt\bar{t}$ which is vastly dominant over $gq\bar{q}t\bar{t}$ and $q\bar{q}t\bar{t}$.

[6]The proper decay length $c\tau_0$ falls within the range from $0.06\mu m$ to $0.19\mu m$, where τ_0 is the light Higgs lifetime at rest [82].

unlike the irreducible backgrounds). We will clearly leverage these underlying partonic shapes in our detector level analysis, to which we proceed next, in the presence of the following sequence of acceptance cuts:

$$p_T^{j,\,b} > 20 \text{ GeV}, \ p_T^l > 10 \text{ GeV}, \ |\eta(l,b)| < 2.5, \ |\eta(j)| < 5.0, \ \Delta R > 0.4$$

BPs	m_h	m_H	m_a	$m_{H^\pm}$	$\sin(\beta-\alpha)$	$\tan\beta$	$\Gamma(h)$	$\Gamma(H)$	$\Gamma(A)$	$\Gamma(H^\pm)$	$\Gamma(Z \to ha)$	σ (pb)
BP1	15.37	125.00	72.21	120.99	-0.19	8.55	3.11×10^{-9}	4.4×10^{-3}	1.028×10^{-4}	7.88×10^{-2}	0.00083	3.28×10^{-4}
BP2	12.56	125.00	74.12	113.93	-0.16	5.97	1.01×10^{-9}	4.4×10^{-3}	1.60×10^{-4}	4.752×10^{-2}	0.000968	4.11×10^{-4}
BP3	11.64	125.00	73.03	104.56	-0.19	5.09	3.13×10^{-9}	4.49×10^{-3}	1.644×10^{-4}	3.96×10^{-2}	0.00164	4.73×10^{-4}

Table 4: Selected BPs with parton level cross section and other observables at LO. (All masses and widths are in GeV.)
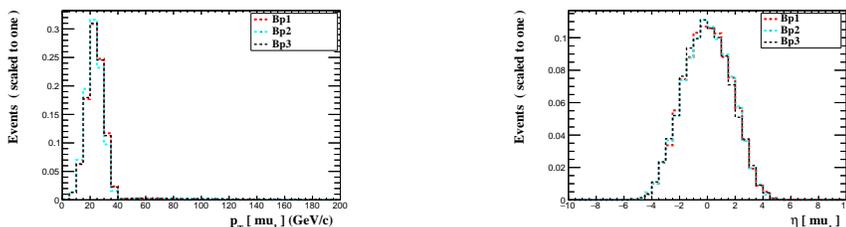
Figure 7: The transverse momentum (left) and pseudorapidity (right) of the hardest muon for the signal (all BPs).
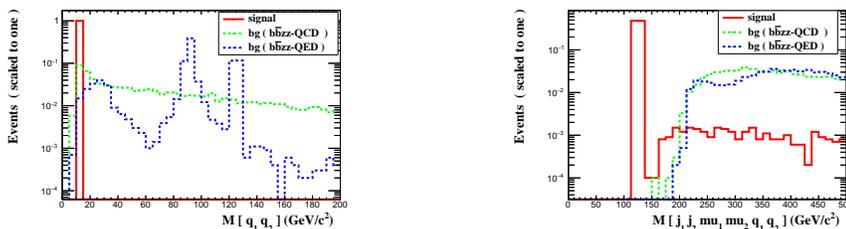
Figure 8: The invariant mass of the $b\bar{b}$ (left) and $\mu^+\mu^-$ jj $b\bar{b}$ (right) system for the signal (BP1) and the two irreducible backgrounds at parton level.

We show in Fig. 9 the distributions of the missing transverse energy ($\not{E}_T$) and the highest p_T's of b-jets, light-jets and muons for signal and background at detector level. (As mentioned previously, the irreducible background stemming from $ZZb\bar{b}$ processes is negligible, so we have not emulated these at detector level.) The $\not{E}_T$ distribution from simulated samples of background events is mainly from di-leptonic decay of $ggt\bar{t}$, i.e., with $t\bar{t} \to W^+bW^-\bar{b} \to (\mu^+\nu_\mu b)(\mu^-\overline{\nu}_\mu\bar{b})$. An interesting observation is the $\not{E}_T$ in the signal, which is given by $H \to aZ^* \to hZ^*Z^* \to \mu^+\mu^-$ jj $b\bar{b}$ events with semi-leptonic b-meson decays (alongside detector effects). Furthermore, Fig. 10 illustrates the different angular separations between b-quarks and muons for signal and background, where one can read that background has only a minimal component with muons coming from semi-leptonic b-meson decays (as intimated).

To enhance the signals and suppress the background from $ggt\bar{t}$, we have adopted several kinematic cuts, which choice is based on comparing different distributions of the signal and background processes at the detector level. Specifically, this has been done through 2D distributions correlating

11
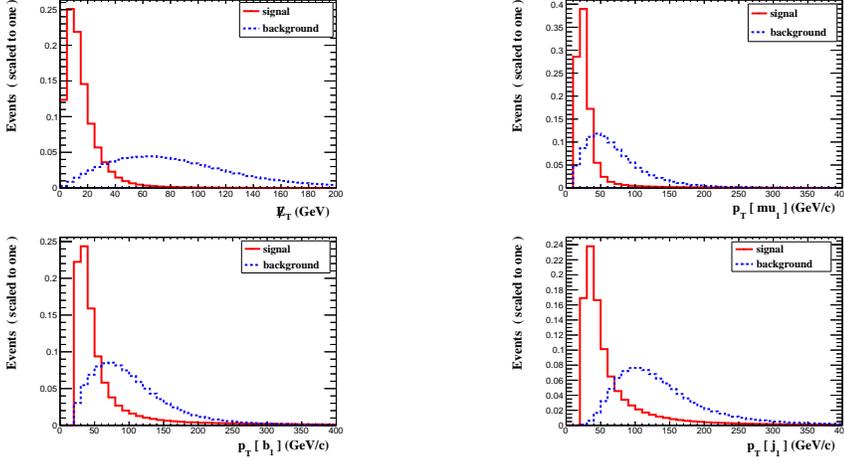
Figure 9: The $\not{E}_T$ and highest p_T distributions for muons, b- and light-jets (clockwise) for signal (BP3) and background (blue) ($ggt\bar{t}$) at detector level.
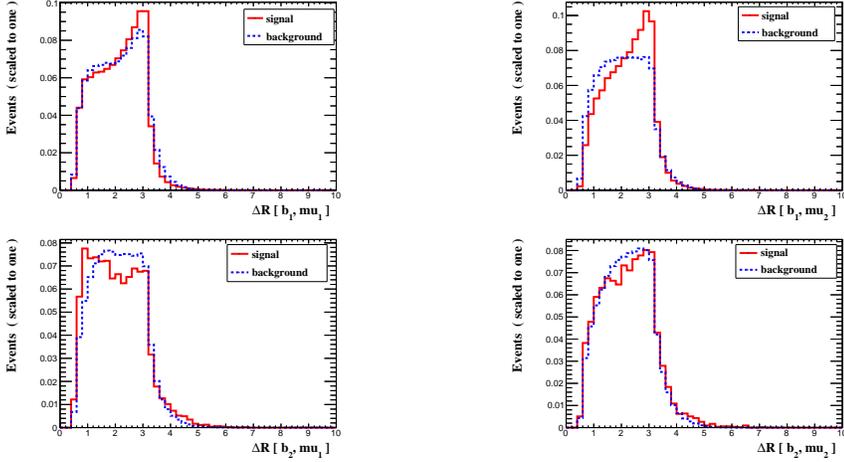
Figure 10: ΔR distributions between the two (p_T ordered) b-jets and muons, from hardest to softest (clockwise) for signal (red) (BP3) and background (blue) at detector level.

the missing transverse momentum to a series of kinematic variables pertaining to some of the visible objects in the final state as illustrated in Figs. 11 and 12 for signal and background, respectively. An interesting observation is that the signal and background distributions are anti-correlated. In fact, it is clear from the left panel of Figs. 11 and 12 that forcing the missing transverse energy to be below 25 GeV will strongly favour the signal over the background. The middle and right panel show that selecting events with $p_T^j < 75$ GeV and $p_T^\mu < 40$ GeV would also enhance the signal significance. Through similar reasoning, further cuts were required on $m_{\mu\mu}$, $\Delta R(b_i, \mu_j)$, $\Delta R(\mu_1, \mu_2)$, $\Delta R(j_1, j_2)$ and $\Delta R(b_1, b_2)$. These selection cuts were finally chosen as follows: $m_{\mu\mu} < 40$ GeV, $\Delta R(b_i, \mu_j) < 2.5$, $\Delta R(\mu_1, \mu_2) < 2.5$, $\Delta R(j_1, j_2) < 2.5$ and $\Delta R(b_1, b_2) < 2.5$.

We have then computed the significance (for $\sqrt{s} = 13$ TeV and $\mathcal{L} = 300$ fb^{-1}), defined as $\Sigma = \frac{S}{\sqrt{B}}$, where $S(B)$ is the signal(background) yield after the discussed cutflow, for not only our three initial BPs (whose Σ rates are 3.20, 4.12 and 4.80 for BP1, BP2 and BP3, respectively), but also those appearing in Tab. 5. We have done so in order to be able to map the 2HDM Type-I parameter space in detail, so as to acquire a sense of the true portion of it that can be tested
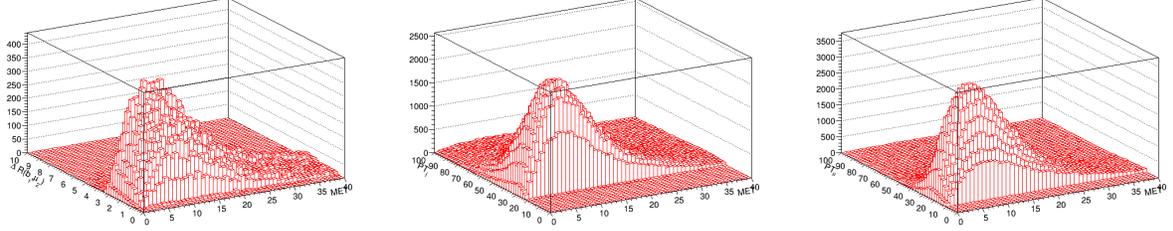
Figure 11: Correlation between $\Delta R(b_1, \mu_2)$ vs. $\not{E}_{\mathrm{T}}$ (left panel), p_T^j vs. $\not{E}_{\mathrm{T}}$ (middle panel) and p_T^μ vs. $\not{E}_{\mathrm{T}}$ (right panel) for the signal (BP3) at detector level.
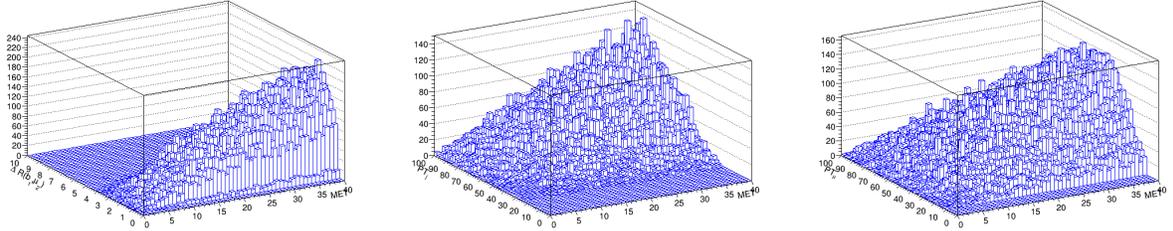
Figure 12: Correlation between $\Delta R(b_1, \mu_2)$ vs. $\not{E}_{\mathrm{T}}$ (left panel), p_T^j vs. $\not{E}_{\mathrm{T}}$ (middle panel) and p_T^μ vs. $\not{E}_{\mathrm{T}}$ (right panel) for the background ($ggt\bar{t}$) at detector level.

by forthcoming experiments. Note that we have kept the same cutflow already illustrated for all such new BPs too. Also, it is at this stage that we take into account the aforementioned QCD K-factors for both signal and background. The applied kinematic cuts can greatly reduce the $ggt\bar{t}$ background, as their efficiency is here $\epsilon = \frac{\text{cross section after cuts}}{\text{cross section before cuts}} = 0.000056$, i.e., much lower than the values associated to all our BPs. Many of the latter can have a significance larger than 3 and up to nearly 5, for Run 3 energy and luminosity. To observe their distribution over the (m_h, m_a) plane, we have finally produced Fig. 13, indeed, assuming $\sqrt{s} = 13$ TeV and $\mathcal{L} = 300$ fb^{-1}, where both Σ and ϵ are mapped. Hence, at Run 3, we can conclude that a substantial portion of the 2HDM Type-I parameter space can offer some evidence (and even near discovery) of the signal we have pursued. Furthermore, we notice that a larger efficiency can be obtained for small m_a: this is because the loss of efficiency with b-tagging is over-compensated by a simultaneous higher efficiency for both j- and μ-tagging. Needless to say, at the HL-LHC, where $\mathcal{L} = 3000$ fb^{-1}, most of the sampled parameter space of the 2HDM Type-I would be discoverable.

5 Conclusions

In this paper, we have shown the outcome of performing some recasting over the parameter space of the 2HDM Type I, wherein the heaviest CP-even Higgs state H is identified with the discovered SM-like one, H_{SM}, while h and a are lighter. After considering the available experimental data from searches for exotic Higgs decay into two light (pseudo)scalars, we have found that the corresponding parameter space for which there is sensitivity via $H_{\mathrm{SM}} \to hh(aa) \to 2b2\tau$ at Run 2 is already excluded by existing constraints from BSM Higgs searches. Furthermore, we have shown that there are regions of the 2HDM Type-I parameter space compliant with theoretical and experimental constraints yielding substantial BR($H^\pm \to W^\pm a$) and BR($H \to Z^* Z^* h$). The large size of the former has been exploited in other literature. Here, concerning the latter, we have made the case for looking at the process $pp \to H_{\mathrm{SM}} \to Z^* A \to Z^* Z^* h$ in $\mu^+ \mu^- jj b\bar{b}$ final states, specifically, in

BP	m_h (GeV)	m_a (GeV)	σ (pb)	K-factor	No. of events	Significance Σ	Efficiency ϵ
BP4	11.85	72.75	4.82×10^{-4}	2.68	10.97	4.88	0.0758
BP5	17.15	76.24	2.54×10^{-4}	2.63	5.254	2.29	0.0689
BP6	24.55	78.85	1.39×10^{-4}	2.62	2.487	1.08	0.059
BP7	15.98	82.43	1.705×10^{-4}	2.63	2.465	1.07	0.048
BP8	34.15	84.26	4.48×10^{-5}	2.60	0.512	0.22	0.038
BP9	20.69	79.30	2.30×10^{-4}	2.63	4.141	1.93	0.068
BP10	16.73	71.67	3.31×10^{-4}	2.63	7.539	3.29	0.0758
BP11	16.78	69.25	3.247×10^{-4}	2.63	7.460	3.26	0.0765
BP12	21.82	85.56	1.42×10^{-4}	2.64	1.455	0.63	0.034
BP13	22.78	77.17	1.629×10^{-4}	2.62	3.144	1.369	0.0643
BP14	17.09	78.40	2.038×10^{-4}	2.63	3.821	1.67	0.062
BP15	19.10	72.89	2.401×10^{-4}	2.62	5.348	2.329	0.074
BP16	15.87	75.024	2.192×10^{-4}	2.62	4.701	2.047	0.0718
BP17	15.67	78.38	2.426×10^{-4}	2.64	4.603	2.02	0.063
BP18	19.76	83.14	1.662×10^{-4}	2.64	2.240	0.98	0.0449
BP19	20.24	76.76	1.873×10^{-4}	2.62	3.740	1.62	0.0665
BP20	28.15	77.04	9.39×10^{-5}	2.61	1.779	0.77	0.063
BP21	27.085	79.40	8.134×10^{-5}	2.61	1.390	0.603	0.056
BP22	11.83	74.06	4.577×10^{-4}	2.69	10.098	4.51	0.073
BP23	12.285	76.51	3.377×10^{-4}	2.63	6.857	2.998	0.067
BP24	13.09	75.47	3.538×10^{-4}	2.65	7.526	3.31	0.0709
BP25	14.15	74.35	3.458×10^{-4}	2.62	7.554	3.29	0.072
BP26	11.96	78.57	3.557×10^{-4}	2.69	6.644	2.97	0.062
BP27	12.60	77.17	3.311×10^{-4}	2.66	6.502	2.87	0.065
BP28	14.30	76.77	2.423×10^{-4}	2.63	5.30	2.31	0.0729
BP29	14.16	78.86	2.572×10^{-4}	2.648	4.795	2.11	0.062
BP30	12.91	81.94	2.004×10^{-4}	2.65	2.991	1.31	0.049
BP31	16.15	81.22	1.843×10^{-4}	2.63	2.917	1.27	0.0527
BP32	12.85	83.93	2.308×10^{-4}	2.66	2.827	1.25	0.0408
BP33	11.63	88.72	1.325×10^{-4}	2.68	0.830	0.369	0.0208
BP34	19.86	88.73	8.03×10^{-5}	2.61	0.502	0.0208	0.021
BP35	22.71	74.16	1.093×10^{-4}	2.61	2.344	1.01	0.071

Table 5: Extended list of BPs used in the MC simulation for the 2HDM Type-I parameter scan, highlighting the h and a masses as well as the signal LO cross section, QCD K-factor and event rate after the full cutflow, together with its significance Σ (against the $t\bar{t}$ background) and efficiency ϵ. Recall that NNLO QCD K-factors have been used for Higgs production (and the NLO QCD one of -27% for $ggt\bar{t}$). Here, $\sqrt{s} = 13$ TeV and $\mathcal{L} = 300$ fb^{-1}.
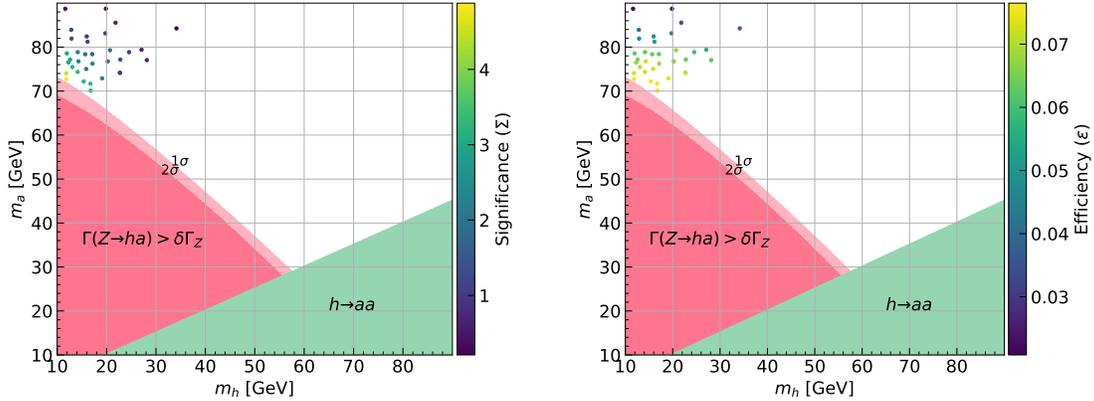
Figure 13: Significance (left) and efficiency (right) of each BP produced in our analysis over the (m_h, m_a) projection of the 2HDM Type-I parameter space, after the full cutflow described in the text.

the region with large m_a and small m_h. After performing a full MC analysis down to detector level, we have proven that the overwhelming background arising from top-quark pair production in association with 2 ISR jets can be suppressed after applying efficient kinematics cuts, leading to a large significance of this hitherto unexplored light Higgs signature already at Run 3 of the LHC, where evidence of it can be seen, further affording one with clear discovery potential at the HL-LHC.

Acknowledgements

References

[1] G. Aad *et al.* [ATLAS and CMS], Phys. Rev. Lett. **114**, 191803 (2015) [arXiv:1503.07589 [hep-ex]].

[2] M. Aaboud *et al.* [ATLAS], Phys. Lett. B **784**, 345-366 (2018) [arXiv:1806.00242 [hep-ex]].

[3] A. M. Sirunyan *et al.* [CMS], JHEP **11**, 047 (2017) [arXiv:1706.09936 [hep-ex]].

[4] G. Aad *et al.* [ATLAS], Eur. Phys. J. C **75**, no.10, 476 (2015) [erratum: Eur. Phys. J. C **76**, no.3, 152 (2016)] [arXiv:1506.05669 [hep-ex]].

[5] M. Aaboud *et al.* [ATLAS], Phys. Lett. B **786**, 223-244 (2018) [arXiv:1808.01191 [hep-ex]].

[6] A. M. Sirunyan *et al.* [CMS], Phys. Rev. D **99**, no.11, 112003 (2019) [arXiv:1901.00174 [hep-ex]].

[7] G. Aad *et al.* [ATLAS and CMS], JHEP **08**, 045 (2016) [arXiv:1606.02266 [hep-ex]].

[8] G. Aad *et al.* [ATLAS], Phys. Rev. D **101**, no.1, 012002 (2020) [arXiv:1909.02845 [hep-ex]].

[9] A. M. Sirunyan *et al.* [CMS], Eur. Phys. J. C **79**, no.5, 421 (2019) [arXiv:1809.10733 [hep-ex]].

[10] [ATLAS], ATLAS-CONF-2021-053.

[11] M. Aaboud *et al.* [ATLAS], Phys. Rev. D **99**, 072001 (2019) [arXiv:1811.08856 [hep-ex]].

[12] [ATLAS], ATLAS-CONF-2020-027.

[13] A. M. Sirunyan *et al.* [CMS], JHEP **07**, 027 (2021) [arXiv:2103.06956 [hep-ex]].

[14] [ATLAS], ATLAS-CONF-2020-026.

[15] A. M. Sirunyan *et al.* [CMS], JHEP **01**, 183 (2019) [arXiv:1807.03825 [hep-ex]].

[16] M. Aaboud *et al.* [ATLAS], Phys. Lett. B **786**, 114-133 (2018) [arXiv:1805.10197 [hep-ex]].

[17] A. M. Sirunyan *et al.* [CMS], Phys. Lett. B **792**, 369-396 (2019) [arXiv:1812.06504 [hep-ex]].

[18] G. Aad *et al.* [ATLAS], Eur. Phys. J. C **80**, no.10, 942 (2020) [arXiv:2004.03969 [hep-ex]].

[19] A. M. Sirunyan *et al.* [CMS], JHEP **03**, 003 (2021) [arXiv:2007.01984 [hep-ex]].

[20] M. Aaboud *et al.* [ATLAS], Phys. Lett. B **789**, 508-529 (2019) [arXiv:1808.09054 [hep-ex]].

[21] A. M. Sirunyan *et al.* [CMS], Phys. Lett. B **791**, 96 (2019) [arXiv:1806.05246 [hep-ex]].

[22] A. M. Sirunyan *et al.* [CMS], Phys. Lett. B **779**, 283-316 (2018) [arXiv:1708.00373 [hep-ex]].

[23] A. Tumasyan *et al.* [CMS], Phys. Rev. Lett. **128**, no.8, 081805 (2022) [arXiv:2107.11486 [hep-ex]].

[24] M. Aaboud *et al.* [ATLAS], JHEP **05**, 141 (2019) [arXiv:1903.04618 [hep-ex]].

[25] G. Aad *et al.* [ATLAS], [arXiv:2111.06712 [hep-ex]].

[26] M. Aaboud *et al.* [ATLAS], Phys. Rev. Lett. **122**, no.23, 231801 (2019) [arXiv:1904.05105 [hep-ex]].

[27] A. M. Sirunyan *et al.* [CMS], Phys. Lett. B **793**, 520-551 (2019) [arXiv:1809.05937 [hep-ex]].

[28] G. Aad *et al.* [ATLAS], [arXiv:2202.07953 [hep-ex]].

[29] M. Grazzini, G. Heinrich, S. Jones, S. Kallweit, M. Kerner, J. M. Lindert and J. Mazzitelli, JHEP **05**, 059 (2018) [arXiv:1803.02463 [hep-ph]].

[30] A. M. Sirunyan *et al.* [CMS], Phys. Lett. B **788**, 7-36 (2019) [arXiv:1806.00408 [hep-ex]].

[31] G. Aad *et al.* [ATLAS], [arXiv:2112.11876 [hep-ex]].

[32] A. M. Sirunyan *et al.* [CMS], Phys. Lett. B **778**, 101-127 (2018) [arXiv:1707.02909 [hep-ex]].

[33] A. Tumasyan *et al.* [CMS], [arXiv:2202.09617 [hep-ex]].

[34] G. Aad *et al.* [ATLAS], Phys. Rev. D **105**, no.9, 092002 (2022) [arXiv:2202.07288 [hep-ex]].

[35] S. Kanemura, T. Kubota and E. Takasugi, Phys. Lett. B **313**, 155-160 (1993) [arXiv:hep-ph/9303263 [hep-ph]].

[36] A. G. Akeroyd, A. Arhrib and E. M. Naimi, Phys. Lett. B **490**, 119-124 (2000) [arXiv:hep-ph/0006035 [hep-ph]]

[37] A. Arhrib, [arXiv:hep-ph/0012353 [hep-ph]].

[38] A. W. El Kaffas, W. Khater, O. M. Ogreid and P. Osland, Nucl. Phys. B **775**, 45-77 (2007) [arXiv:hep-ph/0605142 [hep-ph]].

[39] M. E. Peskin and T. Takeuchi, Phys. Rev. Lett. **65**, 964-967 (1990)

[40] M. E. Peskin and T. Takeuchi, Phys. Rev. D **46**, 381-409 (1992)

[41] P. A. Zyla *et al.* [Particle Data Group], PTEP **2020**, no.8, 083C01 (2020)

[42] D. Eriksson, J. Rathsman and O. Stal, Comput. Phys. Commun. **181**, 189-205 (2010) [arXiv:0902.0851 [hep-ph]].

[43] P. Bechtle, D. Dercks, S. Heinemeyer, T. Klingl, T. Stefaniak, G. Weiglein and J. Wittbrodt, Eur. Phys. J. C **80**, no.12, 1211 (2020) [arXiv:2006.06007 [hep-ph]].

[44] P. Bechtle, S. Heinemeyer, T. Klingl, T. Stefaniak, G. Weiglein and J. Wittbrodt, Eur. Phys. J. C **81**, no.2, 145 (2021) [arXiv:2012.09197 [hep-ph]].

[45] F. Mahmoudi, Comput. Phys. Commun. **180**, 1579-1613 (2009) [arXiv:0808.3144 [hep-ph]].

[46] J. Haller, A. Hoecker, R. Kogler, K. Mönig, T. Peiffer and J. Stelzer, Eur. Phys. J. C **78**, no.8, 675 (2018) [arXiv:1803.01853 [hep-ph]].

[47] R. Aaij *et al.* [LHCb], Phys. Rev. Lett. **118**, no.19, 191801 (2017) [arXiv:1703.05747 [hep-ex]].

[48] Y. Amhis *et al.* [HFLAV], Eur. Phys. J. C **77**, no.12, 895 (2017) [arXiv:1612.07233 [hep-ex]].

[49] A. M. Sirunyan *et al.* [CMS], Phys. Lett. B **795**, 398-423 (2019) [arXiv:1812.06359 [hep-ex]].

[50] M. Aaboud *et al.* [ATLAS], Phys. Lett. B **790**, 1-21 (2019) [arXiv:1807.00539 [hep-ex]].

[51] A. M. Sirunyan *et al.* [CMS], JHEP **11**, 018 (2018) [arXiv:1805.04865 [hep-ex]].

[52] A. M. Sirunyan *et al.* [CMS], Phys. Lett. B **785**, 462 (2018) [arXiv:1805.10191 [hep-ex]].

[53] [CMS], CMS-PAS-HIG-21-003.

[54] P. Uwer, [arXiv:0710.2896 [physics.comp-ph]].

[55] A. M. Sirunyan *et al.* [CMS], JHEP **08**, 139 (2020) [arXiv:2005.08694 [hep-ex]].

[56] G. Aad *et al.* [ATLAS], Phys. Rev. D **105**, no.1, 012006 (2022) [arXiv:2110.00313 [hep-ex]].

[57] A. M. Sirunyan *et al.* [CMS], JHEP **01**, 054 (2018) [arXiv:1708.04188 [hep-ex]].

[58] A. M. Sirunyan *et al.* [CMS], JHEP **10**, 125 (2019) [arXiv:1904.04193 [hep-ex]].

[59] M. Aaboud *et al.* [ATLAS], JHEP **10**, 031 (2018) [arXiv:1806.07355 [hep-ex]].

[60] M. Aaboud *et al.* [ATLAS], JHEP **11**, 040 (2018) [arXiv:1807.04873 [hep-ex]].

[61] [ATLAS], ATLAS-CONF-2021-016.

[62] S. Schael *et al.* [ALEPH, DELPHI, L3, OPAL and LEP Working Group for Higgs Boson Searches], Eur. Phys. J. C **47**, 547-587 (2006) [arXiv:hep-ex/0602042 [hep-ex]].

[63] G. Aad *et al.* [ATLAS], Eur. Phys. J. C **76**, no.4, 210 (2016) [arXiv:1509.05051 [hep-ex]].

[64] S. Semlali, H. Day-Hall, S. Moretti and R. Benbrik, Phys. Lett. B **810**, 135819 (2020) [arXiv:2006.05177 [hep-ph]].

[65] A. Arhrib, R. Benbrik and S. Moretti, Eur. Phys. J. C **77**, no.9, 621 (2017) [arXiv:1607.02402 [hep-ph]].

[66] A. Arhrib, R. Benbrik, M. Krab, B. Manaut, S. Moretti, Y. Wang and Q. S. Yan, JHEP **10** (2021), 073 [arXiv:2106.13656 [hep-ph]].

[67] Y. Wang, A. Arhrib, R. Benbrik, M. Krab, B. Manaut, S. Moretti and Q. S. Yan, JHEP **12**, 021 (2021) [arXiv:2107.01451 [hep-ph]].

[68] [ATLAS], ATLAS-CONF-2021-047.

[69] A. M. Sirunyan *et al.* [CMS], Phys. Rev. Lett. **123**, no.13, 131802 (2019) [arXiv:1905.07453 [hep-ex]].

[70] A. Abulencia *et al.* [CDF], Phys. Rev. Lett. **96**, 042003 (2006) [arXiv:hep-ex/0510065 [hep-ex]].

[71] T. Aaltonen *et al.* [CDF], Phys. Rev. Lett. **107**, 031801 (2011) [arXiv:1104.5701 [hep-ex]].

[72] G. Abbiendi *et al.* [OPAL], Eur. Phys. J. C **72**, 2076 (2012) [arXiv:0812.0267 [hep-ex]].

[73] G. Abbiendi *et al.* [ALEPH, DELPHI, L3, OPAL and LEP], Eur. Phys. J. C **73**, 2463 (2013) [arXiv:1301.6065 [hep-ex]].

[74] R. V. Harlander, S. Liebler and H. Mantler, Comput. Phys. Commun. **184**, 1605-1617 (2013) [arXiv:1212.3249 [hep-ph]].

[75] R. V. Harlander, S. Liebler and H. Mantler, Comput. Phys. Commun. **212**, 239-257 (2017) [arXiv:1605.03190 [hep-ph]].

[76] R. V. Harlander and W. B. Kilgore, Phys. Rev. Lett. **88**, 201801 (2002) [arXiv:hep-ph/0201206 [hep-ph]].

[77] J. Alwall, R. Frederix, S. Frixione, V. Hirschi, F. Maltoni, O. Mattelaer, H. S. Shao, T. Stelzer, P. Torrielli and M. Zaro, JHEP **07**, 079 (2014) [arXiv:1405.0301 [hep-ph]].

[78] G. Bevilacqua, M. Czakon, C. G. Papadopoulos and M. Worek, Phys. Rev. D **84**, 114017 (2011) [arXiv:1108.2851 [hep-ph]].

[79] T. Sjostrand, S. Mrenna and P. Z. Skands, JHEP **05**, 026 (2006) [arXiv:hep-ph/0603175 [hep-ph]].

[80] J. de Favereau *et al.* [DELPHES 3], JHEP **02**, 057 (2014) [arXiv:1307.6346 [hep-ex]].

[81] E. Conte, B. Fuks and G. Serret, Comput. Phys. Commun. **184**, 222-256 (2013) [arXiv:1206.1599 [hep-ph]].

[82] E. Accomando, L. Delle Rose, S. Moretti, E. Olaiya and C. H. Shepherd-Themistocleous, JHEP **04**, 081 (2017) [arXiv:1612.05977 [hep-ph]].

[83] A. M. Sirunyan *et al.* [CMS], JINST **16**, P07001 (2021) [arXiv:2102.04790 [hep-ex]].